Formation of nonequilibrium solid phases by ion irradiation in the Ni-Ta system and their thermodynamic and growth-kinetics interpretations

B. X. Liu and Z. J. Zhang
Department of Materials Science and Engineering, Tsinghua University, Beijing 100084, China and Center of Condensed Matter and Radiation Physics, China Center of Advanced Science and Technology (World Laboratory), Beijing 100080, China
(Received 28 September 1993; revised manuscript received 28 December 1993)

In the Ni-Ta system, several amorphous alloys were synthesized by room-temperature 200-keV xenon-ion irradiation of multilayered films with various compositions. The metallic-glass-forming range was determined experimentally to extend from 25 to 75 at. % Ni. In addition, a hcp metastable crystalline (MC) phase was observed in the Ni-rich $Ni_{80}Ta_{20}$ and $Ni_{75}Ta_{25}$ multilayers at different irradiation stages, and a fcc MC phase was formed in the Ta-rich $Ta_{65}Ni_{25}$ and $Ta_{75}Ni_{35}$ multilayers before and after the films were amorphized, respectively. Interesting evolution behavior of the above nonequilibrium solid phases upon thermal annealing was also observed. A free-energy diagram of the system was constructed based on the model of Miedema, de Boer, and de Boer and the method of Alonso and Simozar. The calculation included the free-energy curves of all the competing phases, especially the MC phases, which were considered as compoundlike, and the enthalpies were calculated based on well-identified structural parameters. The calculated energy sequence of the phases was verified at certain compositions by the phase appearance order in the respective as-deposited multilayers upon steady-state thermal annealing, thus confirming the relevance of the diagram in its general outline. The free-energy diagram can explain the formation and the thermal stability of the above solid phases. The growth kinetics of the hcp and fcc MC phases were also discussed in terms of the structural compatibility between the newly formed phase and the matrix in the ion-irradiation process.

I. INTRODUCTION

In the last ten years, ion-beam mixing has been employed to synthesize metastable materials with either amorphous or crystalline structures.[1-3] Using alternately deposited metals A and B in a multilayered film arrangement, ion-beam mixing can produce A_xB_{1-x} alloys without limitation of composition, as the relative thickness of A and B can be adjusted to obtain arbitrary x from 0 to 1.[4] Ion-beam mixing is commonly considered to be divided into two steps, i.e., the atomic collision cascade and a later step of relaxation, which lasts only for 10^{-10}–10^{-9} sec.[5] By use of a thermal spike, an effective cooling speed as high as 10^{13}–10^{14} K/sec is available in ion-beam mixing. It is thus a very powerful means of synthesizing nonequilibrium solid phases.[6] Up to date, some 70 binary metal systems have been investigated by ion-beam mixing of multilayers,[7] and a great variety of new nonequilibrium solid phases have been synthesized, such as supersaturated solid solutions,[8] metastable Hume-Rothery electron compounds,[9-12] other metastable crystalline phases,[13] and especially a great number of noncrystalline phases or glasses, among which many were not accessible by other synthesis techniques.

With the extensive data obtained, research interest was focused on the formation mechanism of the nonequilibrium phases. Although the amorphization mechanism has not been clarified on an atomic scale due to the complexity of the far-from-equilibrium nature of the ion-solid interactions, several empirical models have been proposed to predict the glass-forming ability of a system from the crystalline structure and other static properties of the constituents and from the features of the equilibrium phase diagram.[14-16] The structural-difference rule proposed by Liu *et al.* in 1983 established the crucial role of the crystalline structures of the constituent metals in determining the structural character of the ion-mixed phases.[17] Later experimental studies[18] have led to a phenomenological model based on two intrinsic parameters: the maximum possible amorphization range, which is defined as 100% minus the maximum solid solubility observed from the corresponding equilibrium phase diagram, and the heat of formation at equiatomic stoichiometry determined by the model of Miedema, de Boer, and de Boer.[19] The prediction of glass-forming ability for binary metal systems by the model is in good agreement with most of the experimental results. Ossi[20] recently established an atomistic model based on the development of the collision cascade and the related bombardment-induced surface compositional change to interpret the nucleation of amorphous or crystalline phase in binary alloys. Using two fundamental parameters, ϕ^*, the work function of the constituent metals, and $n_{WS}^{1/3}$, the electronic density at the boundary of the Wigner-Seitz cell, Ossi plotted a two-dimensional map of the parameters and obtained several lines separating the crystalline and amorphous phase-forming regions. The map can give a reasonable interpretation for some, but not all, of the previously studied systems.

In 1983, Alonso and Simozar proposed a criterion which predicted that amorphous alloys can be formed in systems with a heat of formation less than +10 kJ/mol

but not otherwise.[21] Recently, another method has been developed to calculate the free-energy curves of the competing phases, i.e., solid solutions, amorphous phases, and equilibrium intermetallic compounds, by using a combination of classical elastic theory[22] and the heat of formation.[19] By comparing the free energy of the solid solution and of the amorphous alloy, a quantitative measure of the glass-forming ability can be given.[23] This treatment was quite successful for many systems. However, it cannot explain the formation of various metastable crystalline (MC) phases observed in some alloy systems.[24,25] Besides, it has been argued that the calculation precision of the free energy is doubtful, since the model of Miedema, de Boer, and de Boer[19] and the method of Alonso and Simozar[21] are still semiempirical. Based on current knowledge, however, to give a precise estimation of the errors involved in such a calculation seems quite difficult. We recently proposed an alternative way to conduct the steady-state thermal annealing of the A_xB_{1-x} multilayers to test the relevance of the calculated energies at certain compositions of the competing phases.[26] Since the as-deposited multilayers are in a highly energetic state, they would relax upon annealing to the existing states of the system with lower free energies. The annealing results can thus determine the relative energy levels of the involved phases,[26] especially of the ion-mixed phases concerned.

In this study, the formation of nonequilibrium solid phases in the Ni-Ta system was investigated by ion mixing of multilayers, the free-energy diagram of the system was calculated by a modification of the model of Ref. 19, especially by adding the free-energy curves of the newly observed MC phases, steady-state thermal annealing of the multilayers was conducted to confirm the calculated energy sequence of the phases of interest at some essential compositions, and the growth kinetics of the MC phases were discussed based on a far-from-equilibrium solid-state transition upon ion irradiation. We report, in this paper, the detailed experimental results and the thermodynamic as well as the kinetic interpretation of the formation of the nonequilibrium solid phases.

II. EXPERIMENTAL PROCEDURE

Ni-Ta multilayered films were prepared by alternating deposition of the constituent metals, i.e., pure nickel (99.99% Ni) and tantalum (99.99% Ta), onto a cleaved NaCl single crystal as substrate in a vacuum system. The background vacuum level was on the order of 10^{-7} Torr and it was better than 1×10^{-6} Torr during deposition. Several stoichiometries were selected to cover a wide range of composition, i.e., Ni_{80}, Ni_{75}, Ni_{65}, Ni_{50}, Ni_{40}, Ni_{35}, and Ni_{25}. The substrates were cooled with running water during evaporation and their temperature was estimated to be below 200 °C. The total thickness of the samples was designed to be about 40 nm, which approximately equals the projected range plus the projected range straggling of the irradiation ions, i.e., 200-keV xenon ions. The compositions of the deposited films were controlled by adjusting the relative thicknesses of the constituent metals and were later confirmed by energy-dispersive spectrum (EDS) analysis within an experimental error of 5%. After deposition, the samples were irradiated by 200-keV xenon ions in doses ranging from 1×10^{14} to 5×10^{15} Xe^+/cm^2 at room temperature. The ion-beam current density was controlled to be less than 1 $\mu A/cm^2$ to avoid overheating, and the temperature rise of the films was estimated to be below 100 °C. The vacuum level in the target chamber of the implanter during irradiation was better than 5×10^{-6} Torr. Transmission electron microscopy (TEM) examination, selected area diffraction (SAD), and EDS were used to identify the structures and to determine the exact compositions of the ion-mixed phases. The recrystallization temperatures of the synthesized amorphous alloys and the thermal stability of the observed MC phases were determined, and examined by subsequent annealing with successively increasing temperature in the hot stage of the TEM. The as-deposited multilayered films were also subjected to steady-state thermal annealing in the TEM to give an independent estimate of phase evolution, which was employed to test the validity of the thermodynamic-calculation results for constructing the free-energy diagram.

III. RESULTS AND DISCUSSION

A. Formation of noncrystalline phases

Table I lists the phase changes of Ni-Ta multilayered films under 200-keV xenon-ion mixing at room temperature. From the table, one can see that at the Ni-rich side (i.e., $Ni_{75}Ta_{25}$) the films were amorphized at an irradiation dose of 7×10^{14} Xe^+/cm^2. Figure 1 shows the film

TABLE I. Phase changes of Ni-Ta multilayered films upon room-temperature 200-keV xenon-ion mixing. PA and *A* indicate partial and complete amorphization, respectively; hcp and fcc are two MC phases; while Ni* is a Ni-rich solid solution.

Dose (10^{14} Xe^+/cm^2)	Composition (at. % nickel) Ni_{80}	Ni_{75}	Ni_{65}	Ni_{50}	Ni_{40}	Ni_{35}	Ni_{25}
1	Ni+Ta	Ni+Ta	Ni+Ta	Ni+Ta	Ni+Ta	Ni+Ta	Ni+Ta
3							
5	Ni*	PA					
7	Ni*+hcp	*A*	PA	PA	PA	fcc	PA
10	Ni*+hcp	*A*	PA	PA	PA	fcc	*A*
30		*A*	*A*	*A*	*A*	*A*	*A*
50	hcp	hcp					fcc

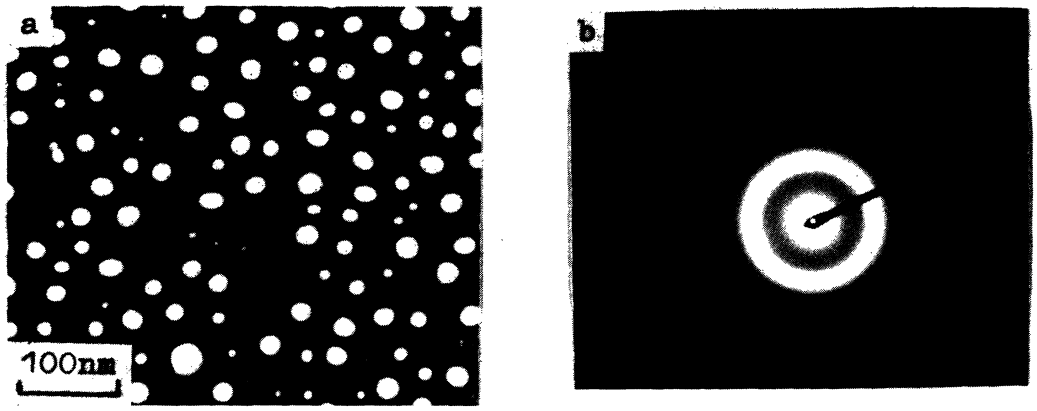

FIG. 1. (a) Morphology and (b) the SAD pattern of the uniform amorphous phase obtained in $Ni_{75}Ta_{25}$ films by room-temperature (RT) 200-keV xenon-ion mixing to a dose of 7×10^{14} Xe^+/cm^2. The scale bar indicates 100 nm.

morphology and the corresponding SAD pattern. At the Ta-rich side, $Ni_{25}Ta_{75}$ films were amorphized at a dose of 1×10^{15} Xe^+/cm^2. Figure 2 illustrates the morphology and the SAD pattern of the amorphized $Ni_{25}Ta_{75}$ films. For all the other studied samples except $Ni_{80}Ta_{20}$ (i.e., $Ni_{65}Ta_{35}$, $Ni_{50}Ta_{50}$, $Ni_{40}Ta_{60}$, and $Ni_{35}Ta_{65}$) the films became amorphous during irradiation (Table I). From these results, it is concluded that the composition range favoring amorphization for the Ni-Ta system may extend at least from 25 to 75 at.% nickel, which is much broader than that observed by other techniques synthesizing noncrystalline phases. The recrystallization temperatures of the ion-mixed amorphous alloys were determined by TEM *in situ* annealing. The recrystallization temperature for the $Ni_{50}Ta_{50}$ amorphous alloy was the highest and was measured to be around 600 °C.

B. Formation and thermal stability of the MC phases

The $Ni_{80}Ta_{20}$ multilayered film changed into a Ni-rich solid solution at an irradiation dose of 5×10^{14} Xe^+/cm^2. Figures 3(a) and 3(b) are the morphology and SAD pattern of the Ni-rich solid solution obtained. When the dose was increased to 7×10^{14} Xe^+/cm^2, some additional sharp diffraction lines emerged and coexisted with those from the Ni-rich solid solution [see Fig. 3(c)]. When the irradiation dose reached 5×10^{15} Xe^+/cm^2, the diffraction lines from the Ni-rich solid solution disappeared and only those new sharp rings were left [Fig. 3(d)]. These lines were identified to be from a new metastable crystalline phase of hcp structure with lattice parameters of $a_{hcp}=2.63$ Å, $c_{hcp}=4.29$ Å, and $c/a=1.63$. Table II gives the indexing of the hcp MC phase. Another Ni-rich sample, (i.e., a $Ni_{75}Ta_{25}$ multilayered film), was amorphized first at a dose of 7×10^{14} Xe^+/cm^2 (see Fig. 1), and irradiation up to a higher dose of 5×10^{15} Xe^+/cm^2 resulted in the formation of the same hcp phase. These results indicate the sensitivity of the phase formation sequence to the chosen composition at the Ni-rich side.

At the Ta-rich side, another new MC phase of fcc structure was observed in both $Ni_{35}Ta_{65}$ and $Ni_{25}Ta_{75}$ multilayered films. The $Ni_{25}Ta_{75}$ multilayered film was first amorphized at a dose of 1×10^{15} Xe^+/cm^2 (see Fig. 2), and then transformed into the fcc MC phase at a dose of 5×10^{15} Xe^+/cm^2, as shown in Fig. 4. Table III lists the indexing for the fcc MC phase; its lattice parameter was $a_{fcc}=4.42$ Å. For the $Ni_{35}Ta_{65}$ film, the fcc MC phase was first observed at a dose of 7×10^{14} Xe^+/cm^2, and amorphization was achieved at a dose of 3×10^{15} Xe^+/cm^2. Obviously, a small compositional difference resulted in a reverse formation sequence for the fcc MC versus the amorphous phase in the above two multilayered films.

To study the thermal stability of the ion-induced MC phases, subsequent *in situ* annealing was carried out and

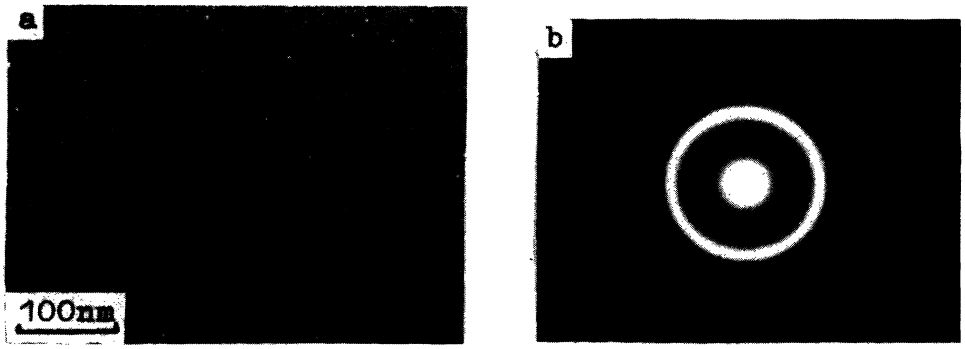

FIG. 2. (a) Bright-field image and (b) the corresponding SAD pattern of the amorphized $Ni_{25}Ta_{75}$ films irradiated by RT 200-keV xenon ions at a dose of 1×10^{15} Xe^+/cm^2. The scale bar indicates 100 nm.

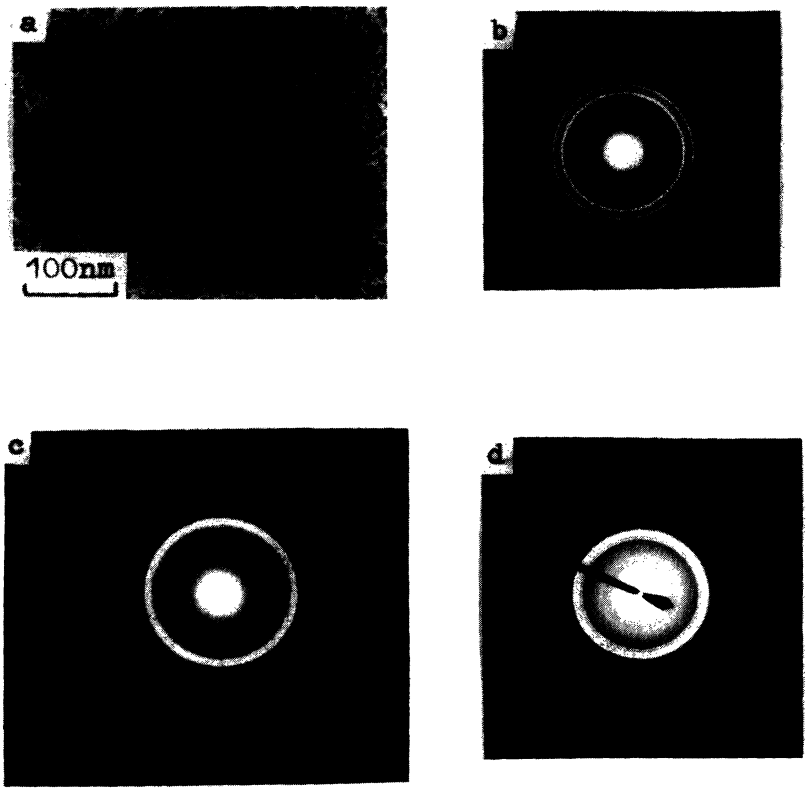

FIG. 3. hcp MC phase formed in $Ni_{80}Ta_{20}$ multilayered films under RT 200-keV xenon-ion mixing. (a) Morphology and (b) the SAD pattern of the Ni-rich solid solution formed in the films at a low irradiation dose of 5×10^{14} Xe^+/cm^2, (c) SAD pattern of the mixture of a Ni-rich solid solution and a hcp MC phase at a higher irradiation dose of 7×10^{14} Xe^+/cm^2, and (d) the SAD pattern of the uniform hcp MC phase at a still higher dose of 5×10^{15} Xe^+/cm^2. The scale bar indicates 100 nm.

some interesting phase evolution sequences were observed. The hcp MC phase formed in the $Ni_{80}Ta_{20}$ multilayered films transformed into a mixture of the hcp phase and a Ni-rich solid solution after annealing at a temperature of 450 °C for 30 min, and then turned into another mixture of the Ni-rich solid solution and the Ta-rich fcc MC phase after annealing at 600 °C for 1 h. Figures 5(a), 5(b), and 5(c) show the SAD patterns of the ion-induced hcp phase, the mixture of the hcp phase plus the Ni-rich solid solution, and the mixture of the Ni-rich solid solution plus the Ta-rich fcc MC phase, respectively. For the $Ni_{75}Ta_{25}$ multilayered films, the hcp phase was stable until 500 °C and then turned into a mixture of the Ni-rich solid solution and the Ta-rich fcc MC phase after annealing at 650 °C for about 40 min. These results can be summarized as

$$\begin{aligned} &\mathrm{hcp}(Ni_{80}Ta_{20}) \underset{30\ \mathrm{min}}{\overset{450\,^\circ\mathrm{C}}{\rightarrow}} \mathrm{hcp}+\mathrm{Ni}^* \underset{60\ \mathrm{min}}{\overset{600\,^\circ\mathrm{C}}{\rightarrow}} \mathrm{fcc}+\mathrm{Ni}^* , \\ &\mathrm{hcp}(Ni_{75}Ta_{25}) \underset{60\ \mathrm{min}}{\overset{500\,^\circ\mathrm{C}}{\rightarrow}} \mathrm{hcp} \underset{40\ \mathrm{min}}{\overset{650\,^\circ\mathrm{C}}{\rightarrow}} \mathrm{fcc}+\mathrm{Ni}^* . \end{aligned} \tag{1}$$

Here, "hcp" and "fcc" represent the two mentioned MC phases, and "Ni*" is the Ni-rich solid solution.

At the Ta-rich side in the $Ni_{25}Ta_{75}$ films, the fcc MC phase was very stable until 650 °C, and then changed into an equilibrium state after annealing at 750 °C for 1 h. In

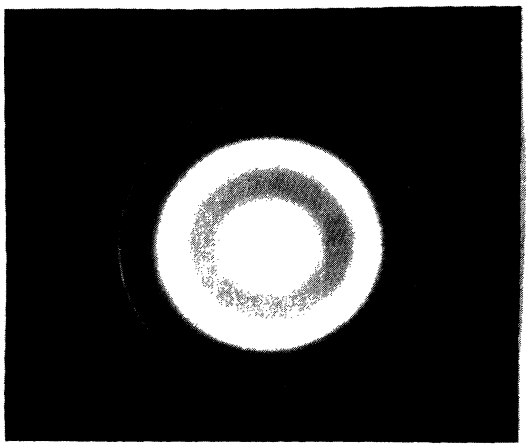

FIG. 4. SAD pattern of the fcc MC phase formed in $Ni_{25}Ta_{75}$ multilayered films by RT 200-keV xenon-ion mixing at a dose of 5×10^{15} Xe^+/cm^2.

TABLE II. Indexing results for the hcp MC phase formed in $Ni_{80}Ta_{20}$ multilayered films by room temperature 200-keV xenon-ion mixing at a dose of 5×10^{15} Xe^+/cm^2. $a=2.63$ Å, $c=4.29$ Å, and $c/a=1.631$.

d_{expt} (Å)	hkl	d_{calc} (Å)	Intensity
2.28	100	2.28	medium
2.14	002	2.14	strong
2.03	101	2.01	strong
1.58	102	1.56	strong
1.30	110	1.32	strong
1.22	103	1.21	medium
1.11	112	1.12	medium
1.08	004	1.07	weak
1.00	104	0.97	weak
0.88	210	0.86	weak

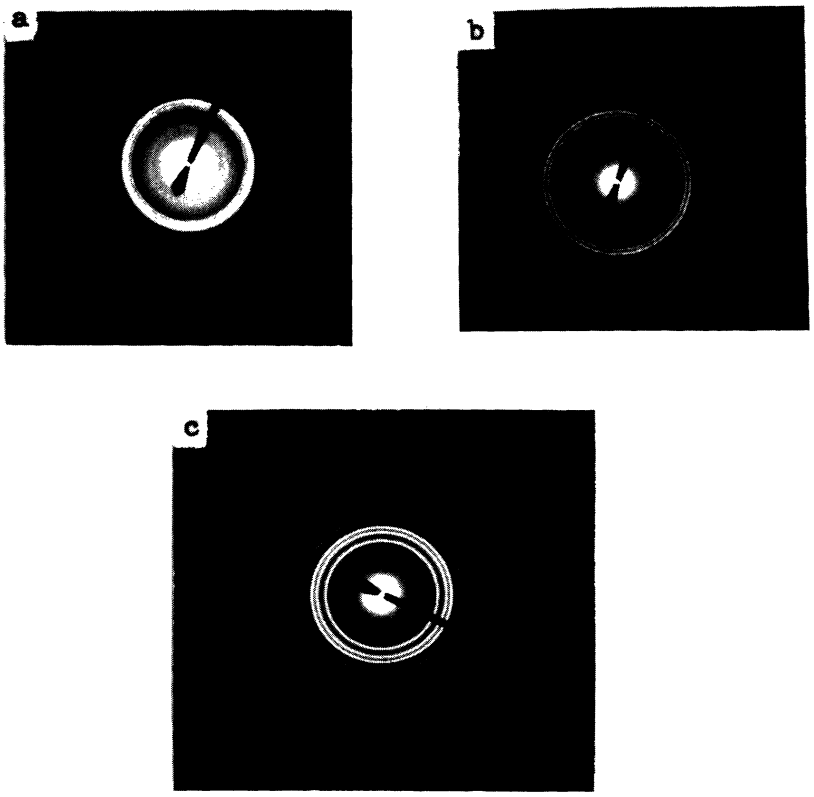

FIG. 5. Thermal stability of the ion-induced hcp MC phase in $Ni_{80}Ta_{20}$ multilayered films. (a) The SAD pattern of the hcp MC phase formed by RT 200-keV xenon mixing at a dose of 5×10^{15} Xe^+/cm^2; (b) after annealing the hcp MC phase at 450 °C for 30 min, the SAD pattern shows the formation of a mixture of the Ni-rich solid solution plus the hcp MC phase; and (c) the SAD pattern of the sample after further annealing at 600 °C for 1 h, showing that a mixture of Ni-rich solid solution plus the Ta-rich fcc MC phase was formed.

the $Ni_{35}Ta_{65}$ films, the fcc MC phase was easily amorphized at 450 °C for 30 min, i.e., the fcc MC phase vitrified. Figure 6 shows its SAD pattern. After further increasing the temperature to 550 °C for about 1 h, a mixture of the Ni-rich solid solution plus the Ta-rich fcc MC phase was observed. These results can be expressed as

$$\begin{aligned} &\text{fcc}(Ni_{35}Ta_{65}) \xrightarrow[30\text{ min}]{450\,^\circ\text{C}} \text{amorphous} \xrightarrow[60\text{ min}]{550\,^\circ\text{C}} \text{fcc}+\text{Ni}^* \ , \\ &\text{fcc}(Ni_{25}Ta_{75}) \xrightarrow[60\text{ min}]{650\,^\circ\text{C}} \text{fcc} \xrightarrow[60\text{ min}]{750\,^\circ\text{C}} \text{equilibrium state} \ . \end{aligned} \tag{2}$$

TABLE III. Indexing results for the fcc MC phase formed in $Ni_{25}Ta_{75}$ multilayered films by room-temperature 200-keV xenon-ion mixing at a dose of 5×10^{15} Xe^+/cm^2. $a=4.42$ Å.

d_{expt} (Å)	hkl	d_{calc} (Å)	Intensity
2.56	111	2.55	strong
2.22	200	2.21	strong
1.55	220	1.56	strong
1.33	311	1.33	strong
1.25	222	1.28	weak
1.07	400	1.10	weak
1.02	331	1.01	medium
0.99	420	0.99	medium
0.91	422	0.90	medium
0.84	511	0.85	weak
0.79	440	0.78	weak
0.72	600	0.74	weak

C. Construction of the free-energy diagram

In general, by comparing the free-energy values of the competing phases, i.e., the solid solutions, the amorphous and MC phases, and the equilibrium compounds, one can gain an understanding of the glass-forming ability and the observed phase evolution. The free-energy change for a given phase can be calculated by $\Delta G=\Delta H-T\Delta S$, where ΔH and ΔS are the enthalpy and entropy changes,

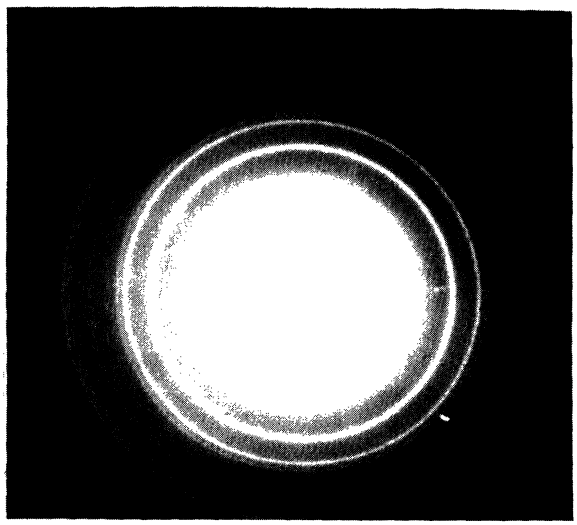

FIG. 6. Upon 450 °C annealing for half an hour, the SAD pattern shows vitrification of the fcc MC phase that was formed in the $Ni_{35}Ta_{65}$ films by RT 200-keV xenon mixing at a dose of 7×10^{14} Xe^+/cm^2.

respectively. The enthalpy and entropy terms can be calculated by the method of Ref. 27, as a function of temperature. However, these thermodynamic data are absent for most known compounds, and no data have been obtained for the MC phases either. The calculation of the free-energy values by this means has thus been difficult.

A "macroscopic atom" model has been developed to calculate the enthalpy values for binary metal alloys.[28–30] In the model, several fundamental parameters were considered, i.e., the work function ϕ^*, the electronic density at the boundary of the Wigner-Seitz cell $n_{\rm WS}^{1/3}$, the atomic size, the valence, and the crystal structures of the components. By using a combination of classical elastic and modern physics theories, the contributions of the above-mentioned factors to the enthalpy were classified into three terms:[31–34] the chemical change due to the electronic interaction when alloying, ΔH_c;[32] the elastic term ΔH_e, which is related to the atomic-size mismatch;[32] and ΔH_s, the structural contribution due to the changes of the number of valence electrons and the crystal structure.[32] Thus the enthalpy change can be expressed by

$$\Delta H = \Delta H_c + \Delta H_e + \Delta H_s \ . \tag{3}$$

Using these considerations, Miedema and co-workers calculated the enthalpy values for most binary transition-metal systems and the results agreed reasonably well with the experimentally determined ones.

Recently, Alonso and co-workers have succeeded in calculating the free-energy change by using this model with some additional assumptions.[35–38] When calculating the free-energy change, the entropy and the enthalpy should be considered together. The enthalpy term can be calculated by the above-mentioned method, while the entropy term is different for the competing phases. For the intermetallic compounds and MC phases, this term was neglected because of the ordered arrangement of the atoms, while for the solid solutions and the amorphous phases, it was simply taken as $\Delta S = -R(x_A \ln x_A + x_B \ln x_B)$, where R is the gas constant and x_A and x_B are atomic concentrations of metals A and B, like that of an ideal solid solution as a first approximation. Therefore, the free-energy change can be written as, taking the solid solution for an example,

$$\Delta G_s = \Delta H_s^c + \Delta H_s^e + \Delta H_s^s - T\Delta S \ . \tag{4}$$

Using this calculation method, some free-energy diagrams have been constructed which gave a reasonable interpretation of the glass-forming ability and spontaneous vitrification in some binary metal systems.[39–42] However, the calculation of $\Delta G_{\rm MC}$ was not successful for the ion-mixed MC phases.[24,25]

To our knowledge, a free-energy calculation has not been successfully performed for the ion-mixed MC phases so far. Since two types of MC phases have been synthesized by ion-beam mixing in this study and their structures have been identified, the calculation of these two phases becomes possible upon some reasonable assumptions. It should be pointed out that the composition of the hcp MC phase was at the Ni-rich (fcc) side and close to an equilibrium compound of complicated structure, while the composition of the fcc MC phase was at the Ta-rich (bcc) side and near to the eutectic point, corresponding to no complicated compound. Besides, according to Ref. 32, at the fcc (or hcp) metal side, the most stable structure of a MC phase is hcp or fcc, while for the bcc metal side, it is bcc. In other words, the structure of the hcp MC phase was favored by its composition, while the structure of the fcc MC was not.

We now discuss the calculation method for the MC phase in detail. First, the hcp and fcc MC phases were both of ordered structure and can be considered as compoundlike. It follows that the chemical contributions and entropy terms can be calculated as for an equilibrium compound by Eq. (4). However, the crystalline structure and the atomic arrangement of the MC phases are different from those of the equilibrium compound, which results in additional elastic and structural contributions to the enthalpy of the MC phases. Considering the hcp MC phase formed near the position of the equilibrium compound, the elastic term should be calculated by the model of Ref. 32, since the atomic arrangement in the MC phase is different from that in the compound, and the elastic energy cannot be relaxed to zero as in the compound. For the fcc MC phase formed in the vicinity of

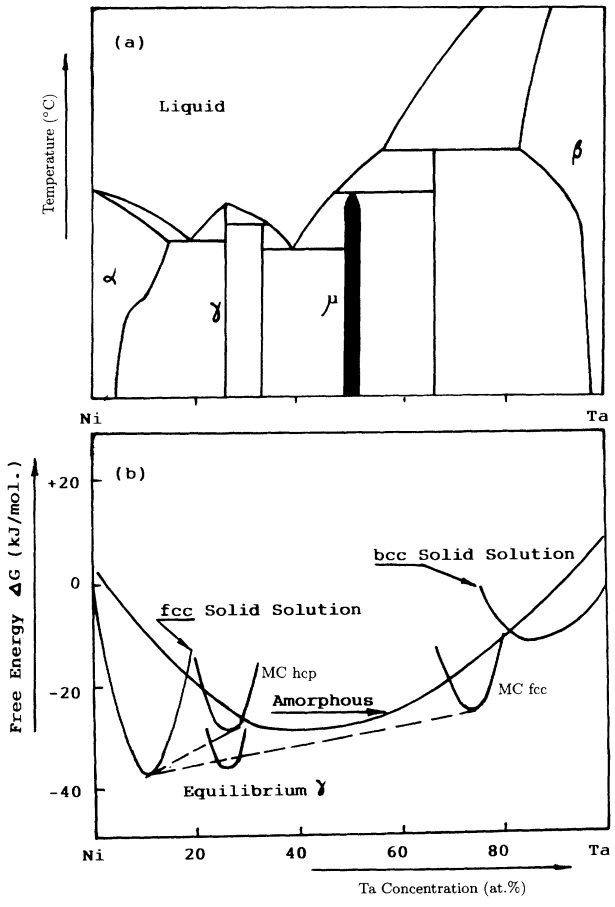

FIG. 7. (a) Equilibrium phase diagram and (b) calculated Gibbs free-energy diagram of the Ni-Ta system. The dashed lines show the cotangent lines, where some intermediate states are situated during thermal annealing.

the eutectic point where no corresponding equilibrium compound exists, the elastic term can be neglected because the ordered arrangement of the atoms can relax to a minimum lattice distortion caused by the atomic-size mismatch of the constituent metals. This distortion was indeed calculated to be negligible according to the method proposed by Jawson and Wheeler.[43] Thus, for a MC phase formed at the composition of an equilibrium compound,

$$\Delta G_{\mathrm{MC}}=\Delta H^{c}_{\mathrm{MC}}+\Delta H^{e}_{\mathrm{MC}}+\Delta H^{s}_{\mathrm{MC}} , \tag{5}$$

and for the other type of MC phase,

$$\Delta G_{\mathrm{MC}}=\Delta H^{c}_{\mathrm{MC}}+\Delta H^{s}_{\mathrm{MC}} . \tag{6}$$

Figures 7(a) and 7(b) show the equilibrium phase diagram and the calculated free-energy diagram (at 300 K as a typical example) for the Ni-Ta system. It should be noted that, in the free-energy diagram, the free-energy curves for the solid solutions and the amorphous phases were calculated by the method described above, while for the equilibrium intermetallic compounds and the MC phases, only the minimum values were actually given by the calculation. The free-energy curves of the two MC phases are schematically narrow because they are considered as compoundlike.

D. Discussion

1. *Thermal annealing to confirm the relative energies*

Steady-state thermal annealing of some as-deposited films was conducted with increasing temperature. In the $Ni_{80}Ta_{20}$ films, the hcp phase was formed after annealing at 300 °C for 30 min. When the temperature was increased to 400 °C for 30 min, the hcp phase turned into a mixture of the hcp phase and the Ni-rich solid solution. Further annealing at 500 °C for 30 min resulted in the formation of a mixture of the Ni-rich solid solution and the Ta-rich fcc MC phase. In the $Ni_{75}Ta_{25}$ films, the amorphous phase was first observed after annealing at 400 °C for 1 h and then changed into the hcp phase after annealing at 500 °C for 30 min. When the temperature was raised to 700 °C for 20 min, the hcp MC phase transformed into a mixture of the Ni-rich solid solution and the Ta-rich fcc MC phase. It is worth mentioning that the lattice parameters of the hcp and fcc MC phases formed by thermal annealing and ion irradiation are not very different. The phase evolution in the Ni-rich multilayers upon annealing can be summarized as follows,

$$\begin{aligned}&\mathrm{Ni_{80}Ta_{20}} \xrightarrow[30\ \mathrm{min}]{300\,^{\circ}\mathrm{C}} \mathrm{hcp} \xrightarrow[30\ \mathrm{min}]{400\,^{\circ}\mathrm{C}} \mathrm{hcp+Ni^{*}} \xrightarrow[30\ \mathrm{min}]{500\,^{\circ}\mathrm{C}} \mathrm{fcc+Ni^{*}} ,\\ &\mathrm{Ni_{75}Ta_{25}} \xrightarrow[60\ \mathrm{min}]{400\,^{\circ}\mathrm{C}} \mathrm{amorphous} \xrightarrow[30\ \mathrm{min}]{500\,^{\circ}\mathrm{C}} \mathrm{hcp} \xrightarrow[20\ \mathrm{min}]{700\,^{\circ}\mathrm{C}} \mathrm{fcc+Ni^{*}} .\end{aligned} \tag{7}$$

Here, "hcp" and "fcc" are the two MC phases, and "Ni*" is the Ni-rich solid solution.

In the $Ni_{35}Ta_{65}$ films, the fcc MC phase was first obtained after annealing at 350 °C for 30 min and then turned amorphous at 450 °C; further increase in temperature to 500 °C caused the transformation of the amorphous phase into a mixture of the fcc MC phase plus the Ni-rich solid solution. For the $Ni_{25}Ta_{75}$ films, amorphization occurred first after annealing at 400 °C for 1 h, and then it changed into the fcc MC phase after annealing at a higher temperature of 500 °C for 20 min. When the annealing temperature was increased to 750 °C for an hour, the film changed into the equilibrium phase. The phase evolution in Ta-rich multilayer upon thermal annealing can be summarized as follows,

$$\begin{aligned}&\mathrm{Ni_{35}Ta_{65}} \xrightarrow[30\ \mathrm{min}]{350\,^{\circ}\mathrm{C}} \mathrm{fcc} \xrightarrow[60\ \mathrm{min}]{450\,^{\circ}\mathrm{C}} \mathrm{amorphous} \xrightarrow[30\ \mathrm{min}]{500\,^{\circ}\mathrm{C}} \mathrm{fcc+Ni^{*}} ,\\ &\mathrm{Ni_{25}Ta_{75}} \xrightarrow[60\ \mathrm{min}]{400\,^{\circ}\mathrm{C}} \mathrm{amorphous} \xrightarrow[20\ \mathrm{min}]{500\,^{\circ}\mathrm{C}} \mathrm{fcc} \xrightarrow[60\ \mathrm{min}]{750\,^{\circ}\mathrm{C}} \text{equilibrium state} .\end{aligned} \tag{8}$$

From these phase appearance sequences upon steady-state thermal annealing, it is revealed that the free energies of the hcp and fcc MC phases can be either lower or higher than that of the amorphous phase, depending on the alloy composition. This suggests that the free-energy curves of the hcp MC phase versus the amorphous phase and the fcc MC phase versus the amorphous phase should intersect each other along the composition axis. In the constructed free-energy diagram shown in Fig. 7(b), the calculated free-energy curves were arranged in a configuration with exactly the same energy sequence of the related phases as that observed by thermal-annealing experiments. It is therefore believed that the calculated free-energy diagram is relevant in its general outline, though calculation of the precise energy differences among the related phases should be improved and requires further studies.

2. *Interpretation of the phase formation and evolution*

In Fig. 7(b), the free-energy curve of the amorphous phase is lower than those of the two terminal solid solutions within a broad composition range of 18–82 at. % nickel. Simply taking this range as a measure of the glass-forming ability, the composition range favoring amorphization for the Ni-Ta system is therefore from 18 to 82 at. % nickel, which is in good agreement with the range revealed by ion-mixing experiments, i.e., 25–75 at. % nickel.

The formation of two MC phases in this system can also be well explained by the calculated free-energy diagram. For the fcc MC phase formed at the Ta-rich side, one sees from the free-energy diagram that the free energy of the fcc phase for $Ni_{25}Ta_{75}$ is more negative than that of the amorphous phase, while the free energy of the same fcc MC phase for $Ni_{35}Ta_{65}$ is more positive than that of the amorphous phase. It is then expected that, with increasing ion doses, the amorphous phase would emerge first in the $Ni_{25}Ta_{75}$ films and then the fcc MC phase, and that in the $Ni_{35}Ta_{65}$ films, the formation sequence would be just the contrary. This was indeed the case with the experimental results reported in Sec. III B 1. For the hcp phase formed at the Ni-rich end, one sees from Fig. 7(b) that for $Ni_{75}Ta_{25}$ it is more stable than

the amorphous phase, while the amorphous phase is more stable than the hcp phase for $Ni_{80}Ta_{20}$. In the ion-mixing experiments, the amorphous phase was first formed in the $Ni_{75}Ta_{25}$ films and then transformed into the hcp phase, which agrees with the expectation of the calculated diagram. However, for the $Ni_{80}Ta_{20}$ films, no amorphous phase was observed at any irradiation doses used. Instead, a fcc Ni-rich solid solution was formed at low doses, and then transformed into the hcp MC phase upon further irradiation. This is because it is easy to transform from the fcc to the hcp structure in the ion-irradiation process (to be discussed later), so that no amorphous phase was formed in the experiment.

The phase evolution of the MC phases upon thermal annealing can also be well explained. According to Fig. 7(b), when the hcp MC phase in the $Ni_{80}Ta_{20}$ films is annealed with successively increasing temperature, it should evolve in the following sequence: hcp$\rightarrow$hcp+Ni*$\rightarrow$fcc+Ni*, which is indeed the case experimentally (Sec. III B 2). For the fcc MC phase formed in the $Ni_{35}Ta_{65}$ films, the transition sequence upon thermal annealing can also be deduced from Fig. 7(b) as fcc$\rightarrow$amorphous$\rightarrow$fcc+Ni*, which also agrees well with the experimental results (see Sec. III B 2).

IV. KINETIC MODELS

The above calculations confirmed the thermodynamic driving force for the formation of the two MC phases. The next question is then how the growth kinetics of the new phases proceed under ion-beam mixing. It is well known that ion-beam mixing can generally be divided into two steps, first an atomic collision cascade and then a relaxation period lasting only for 10^{-10}–10^{-9} sec, within which the newly formed phase is expected to grow. As a consequence, the alloy phase formed upon ion irradiation can only be of a simple crystalline structure or disordered, namely amorphous, because such a short span of time prevents the nucleation and growth of a complicated structured phase, as long-range diffusion is impossible.[44] Accordingly, only fast and partitionless transition mechanisms can occur. It is commonly accepted that the phase transformation induced by ion irradiation in thin solid films is a solid-solid transition. The structural compatibility between the newly formed phase and the matrix therefore frequently plays an important role in determining whether the new phase can grow or not.[45]

In our case, the hcp MC phase was formed based on the Ni-rich solid solution (fcc), while the fcc MC phase was formed from the Ta-rich (bcc) solid solution. For the hcp MC phase, as the hcp and fcc structures are quite similar, the transition fcc$\rightarrow$hcp can be easily realized by a sliding on the $(111)_{fcc}$ plane along the $[11\bar{2}]_{fcc}$ direction by a vector of $\frac{1}{3}[11\bar{2}]_{fcc}$. From this sliding mechanism, the relationship between the two lattices can be deduced as $a_{hcp}=\sqrt{2}/2a_{fcc}$. At the composition $Ni_{80}Ta_{20}$, the lattice parameter of the Ni-rich solid solution can be calculated by Vegard's law as $a_{fcc}=3.66$ Å, which results in an $a_{hcp}=2.59$ Å. Compared with the experimental value of $a_{hcp}=2.63$ Å, the difference is less than 2%.

Generally speaking, direct transformation from the bcc to the fcc structure is somewhat difficult and has scarcely been induced in thin films by ion irradiation. It is therefore believed that the formation of the fcc MC phase in $Ni_{35}Ta_{65}$ multilayers was by a two-step transition process, i.e., from the bcc structure of the Ta matrix first to an intermediate state of hexagonal structure and then to fcc. If the bcc structure first transforms into a hexagonal structure, the fcc MC phase can then be formed from the transition hcp$\rightarrow$fcc. The assumed two-step transition mechanism leads to a lattice-parameter relationship of $a_{fcc}=\sqrt{6}/2a_{bcc}$. Using the lattice parameter of pure tantalum of 3.31 Å, the lattice parameter of the fcc phase was calculated to be 4.05 Å. As mentioned in Sec. III B, the lattice parameter of the ion-mixed fcc MC phase was 4.42 Å. The difference between the calculated and the experimental values is close to the errors involved. In fact, we have recently observed such a two-step phase transition in the Ni-Nb, Co-Nb, and Fe-Nb systems; especially, the intermediate state of hexagonal structure has been experimentally detected,[46] which lends strong support to the above interpretation of the formation of the fcc MC phase in the $Ni_{25}Ta_{75}$ multilayers. It is of interest that the formation of the fcc MC phase in the $Ni_{25}Ta_{75}$ multilayers was different, because the fcc phase was not formed from Ta crystal, but from a previously mixed amorphous matrix. According to an estimate of the atomic movement during relaxation, nucleation of simple-structured clusters is possible up to a size of 30 Å.[44] The growth of the fcc phase is thus thought to proceed through a typical nucleation and growth process in a liquidlike amorphous matrix.

V. CONCLUDING REMARKS

(1) Amorphization was achieved in the Ni-Ta system by RT 200-keV xenon-ion mixing, and the glass-forming range was quantitatively determined to extend through a wide composition range of 25–75 at. % nickel. In addition, two MC phases were synthesized by ion mixing, one of fcc structure at the Ta-rich side and the other of hcp structure at the Ni-rich end.

(2) A Gibbs free-energy diagram of the Ni-Ta system was established by calculating the free-energy curves of the observed phases on the basis of the theory of heats of formation of Miedema, de Boer, and de Boer[19] and the calculation method of Alonso and Simozar[21], in which the free-energy curves of the two MC phases were included.

(3) Steady-state thermal annealing of the as-deposited Ni-Ta multilayered films in which the two MC were observed under ion mixing was conducted. The annealing results for these films showed the same energy sequence as that revealed by the calculated diagram, and thus confirmed the relevance of the calculation.

(4) The calculated diagram gave a measure of the glass-forming ability of the system for 18–82 at. % nickel, which agreed well with the experimental results. The

observed phase formation and evolution can also be explained by the calculated phase diagram.

(5) The formation kinetics of the MC phases were considered to proceed through some fast solid-solid transition mechanisms and the deduced lattice parameters of the phases were in agreement with the experimental ones.

ACKNOWLEDGMENTS

The authors are grateful to the researchers in the Transmission Electron Microscopy Laboratory of Peking University and the Analysis Center of Tsinghua University for their help. Partial financial aid from the National Natural Science Foundation of China is also appreciated.

[1]B. X. Liu, Nucl. Instrum. Methods Phys. Res. Sect. B **40/41**, 608 (1989).
[2]G. Was, Prog. Surf. Sci. **32**, 211 (1989).
[3]M. Nastasi and J. W. Mayer, Mater. Sci. Rep. **9**, 1 (1991).
[4]B. X. Liu, Phys. Status Solidi A **94**, 11 (1986).
[5]M. V. Thompson, *Defects and Radiation Damage in Metals* (Cambridge University, Cambridge, 1969), Chaps. 4 and 5.
[6]L. S. Hung, M. Nastasi, J. Gyulai, and J. W. Mayer, Appl. Phys. Lett. **42**, 672 (1983).
[7]B. X. Liu, Vacuum **42**, 75 (1991).
[8]B. Y. Tasur, S. S. Lau, L. S. Hung, and J. W. Mayer, Nucl. Instrum. Methods **182/183**, 67 (1981).
[9]K. T-Y. Kung, B. X. Liu, and M. A. Nicolet, Phys. Status Solidi A **77**, 355 (1983).
[10]B. X. Liu, D. Z. Che, Z. J. Zhång, S. L. Lai, and J. R. Ding, Phys. Status Solidi A **128**, 345 (1991).
[11]B. X. Liu and M. A. Nicolet, Thin Solid Films **101**, 201 (1983).
[12]B. X. Liu, M. A. Nicolet, and S. S. Lau, Phys. Status Solidi A **73**, 183 (1983).
[13]D. E. Follstaedt, Nucl. Instrum. Methods Phys. Res. Sect. B **7/8**, 11 (1985).
[14]C. L. Chien, Phys. Rev. B **33**, 3243 (1986).
[15]K. Affolter, M. V. Allmen, H. P. Weber, and M. Wittmer, J. Non-Cryst. Solids **55**, 387 (1983).
[16]S. Simozar and J. A. Alonso, Phys. Status Solidi A **81**, 55 (1984).
[17]B. X. Liu, W. L. Johnson, M. A. Nicolet, and S. S. Lau, Appl. Phys. Lett. **42**, 45 (1983).
[18]B. X. Liu, Mater. Lett. **5**, 322 (1987).
[19]A. R. Miedema, F. R. de Boer, and P. F. de Boer, J. Phys. F **3**, 1558 (1983).
[20]P. M. Ossi, Phys. Status Solidi A **119**, 463 (1990).
[21]J. A. Alonso and S. Simozar, Solid State Commun. **46**, 765 (1983).
[22]J. D. Eshelby, Solid State Phys. **3**, 79 (1956).
[23]L. J. Gallego, J. A. Somoza, J. A. Alonso, and J. M. Lopez, Physica B **154**, 82 (1988).
[24]A. Blatter, J. Gfeller, and M. V. Allmen, J. Less-Common Met. **140**, 317 (1988).
[25]H. Schliiter, H. C. Freyhart, H. V. Kres, and R. Bormann, Z. Phys. Chem. Abt. A **157**, 407 (1988).
[26]Z. J. Zhang and B. X. Liu, J. Phys.: Condens. Matter (to be published).
[27]A. K. Neissen, F. R. de Boer, R. Boom, P. F. de Chatel, W. C. M. Mattens, and A. R. Miedema, CALPHAD: Comput. Coupling Phase Diagrams Thermochem. **7**, 51 (1983).
[28]J. R. Chelikowsky and J. C. Phillips, Phys. Rev. B **17**, 2453 (1978).
[29]J. A. Alonso and L. A. Girifalco, J. Phys. F **8**, 2455 (1978).
[30]A. R. Williams, C. D. Gelatt, and V. L. Moruzzi, Phys. Rev. Lett. **44**, 429 (1980).
[31]A. R. Miedema, P. F. de Chatel, and F. R. de Boer, Physica B **100**, 1 (1988).
[32]A. K. Niessen and A. R. Miedema, Ber. Bunsenges. Phys. Chem. **87**, 717 (1983).
[33]A. K. Niessen, A. R. Miedema, F. R. de Boer, and R. Boom, Physica B **151**, 401 (1988).
[34]F. R. de Boer, R. Boom, W. C. M. Matters, A. R. Miedema, and A. K. Niessen, *Cohesion in Metals: Transition Metal Alloys* (North-Holland, Amsterdam, 1988).
[35]J. A. Alonso, L. J. Gallego, and J. M. Lopez, Philos. Mag. A **58**, 79 (1988).
[36]J. M. Lopez, J. A. Alonso, and L. J. Gallego, Phys. Rev. B **36**, 3716 (1987).
[37]L. Gallego, J. S. Simozar, J. A. Alonso, and J. M. Lopez, J. Phys. F **18**, 2149 (1988).
[38]J. A. Alonso, L. J. Gallego, and J. A. Simozar, Nuovo Cimento **12**, 587 (1990).
[39]M. V. Allmen and A. Blatter, Appl. Phys. Lett. **50**, 1873 (1987).
[40]J. A. Alonso, L. J. Gallego, J. A. Simozar, and B. X. Liu, in *Thin Films and Beams-Solid Interactions,* edited by L. J. Huang (Elsevier, Amsterdam, 1991), p. 297.
[41]L. G. Gallego, J. A. Somoza, H. M. Fernandez, and J. A. Alonso, in *Ordering and Disordering in Alloys,* edited by A. R. Yavari (Elsevier, London, 1992), p. 328.
[42]B. X. Liu, H. Y. Bai, Z. J. Zhang, and Q. L. Qiu, J. Alloys Compounds **196**, 37 (1993).
[43]M. A. Jawson and J. A. Wheeler, Acta Crystallogr. **1**, 216 (1948).
[44]B. X. Liu, W. L. Johnson, M. A. Nicolet, and S. S. Lau, Nucl. Instrum. Methods Phys. Res. **209/210**, 229 (1983).
[45]X. Zhou, H. K. Dong, H. D. Li, and B. X. Liu, J. Appl. Phys. **63**, 4942 (1988).
[46]B. X. Liu and Z. J. Zhang, J. Mater. Res. **9**, 357 (1994).

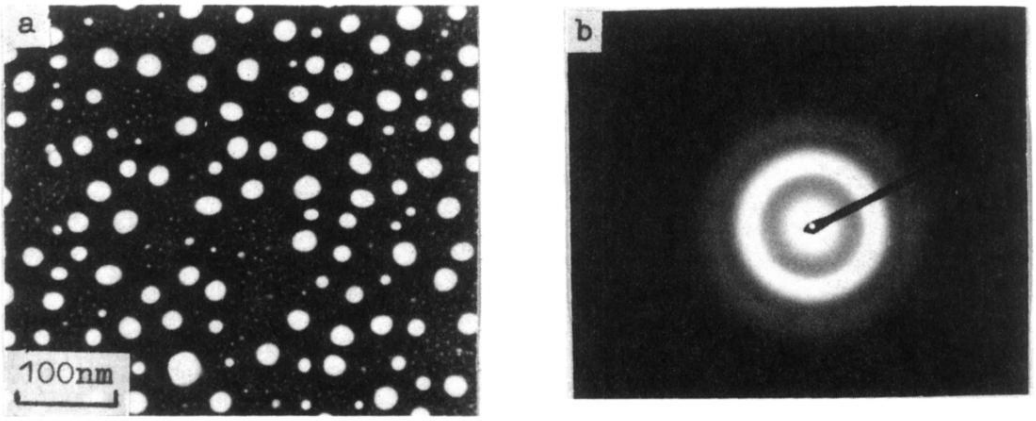

FIG. 1. (a) Morphology and (b) the SAD pattern of the uniform amorphous phase obtained in $Ni_{75}Ta_{25}$ films by room-temperature (RT) 200-keV xenon-ion mixing to a dose of 7×10^{14} Xe^{+}/cm^{2}. The scale bar indicates 100 nm.

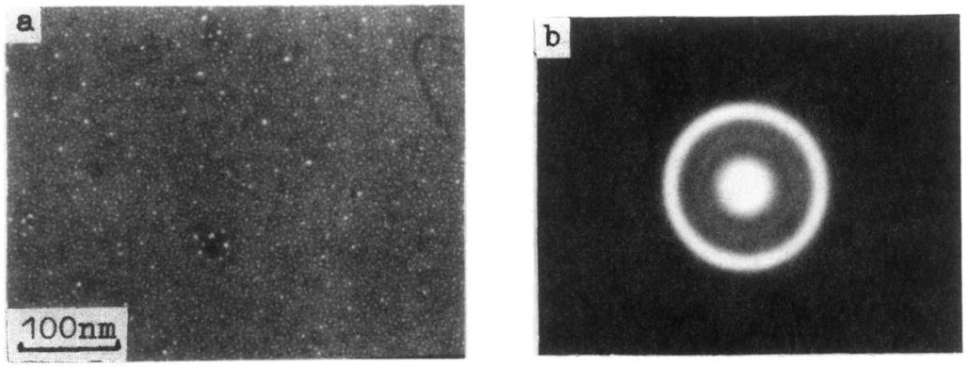

FIG. 2. (a) Bright-field image and (b) the corresponding SAD pattern of the amorphized $Ni_{25}Ta_{75}$ films irradiated by RT 200-keV xenon ions at a dose of 1×10^{15} Xe^{+}/cm^{2}. The scale bar indicates 100 nm.

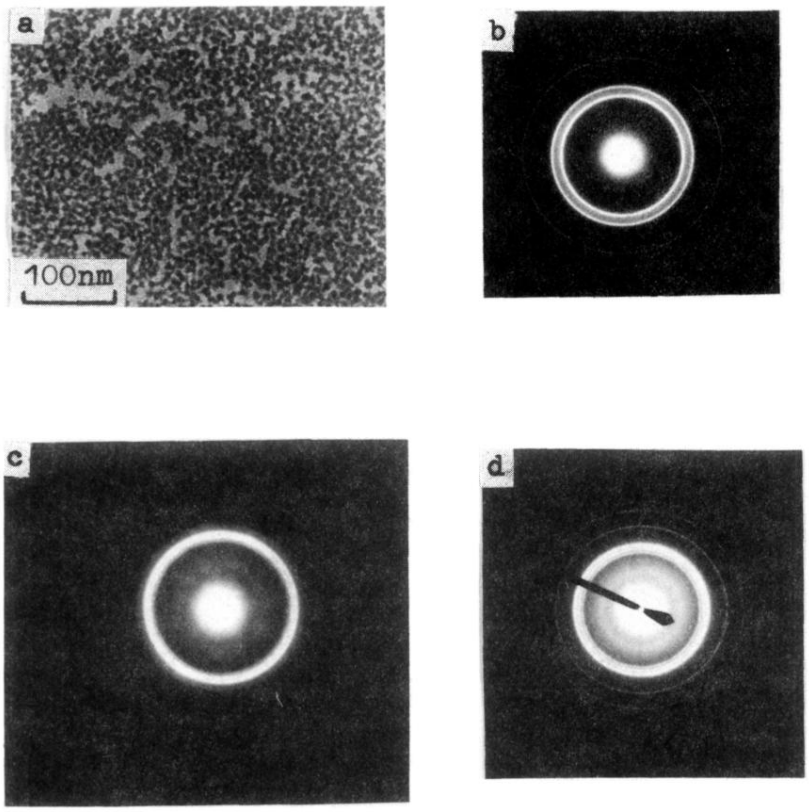

FIG. 3. hcp MC phase formed in $Ni_{80}Ta_{20}$ multilayered films under RT 200-keV xenon-ion mixing. (a) Morphology and (b) the SAD pattern of the Ni-rich solid solution formed in the films at a low irradiation dose of 5×10^{14} Xe^{+}/cm^{2}, (c) SAD pattern of the mixture of a Ni-rich solid solution and a hcp MC phase at a higher irradiation dose of 7×10^{14} Xe^{+}/cm^{2}, and (d) the SAD pattern of the uniform hcp MC phase at a still higher dose of 5×10^{15} Xe^{+}/cm^{2}. The scale bar indicates 100 nm.

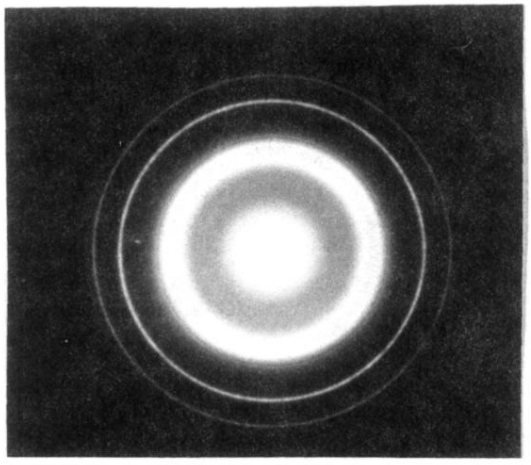

FIG. 4. SAD pattern of the fcc MC phase formed in $Ni_{25}Ta_{75}$ multilayered films by RT 200-keV xenon-ion mixing at a dose of 5×10^{15} Xe^{+}/cm^{2}.

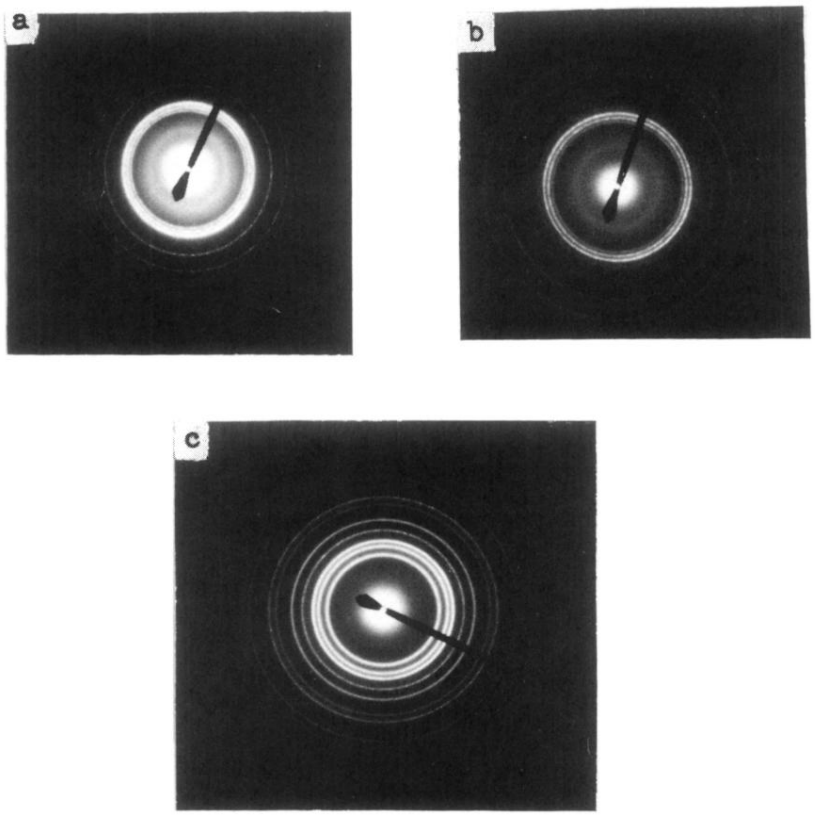

FIG. 5. Thermal stability of the ion-induced hcp MC phase in $Ni_{80}Ta_{20}$ multilayered films. (a) The SAD pattern of the hcp MC phase formed by RT 200-keV xenon mixing at a dose of 5×10^{15} Xe^{+}/cm^{2}; (b) after annealing the hcp MC phase at 450 °C for 30 min, the SAD pattern shows the formation of a mixture of the Ni-rich solid solution plus the hcp MC phase; and (c) the SAD pattern of the sample after further annealing at 600 °C for 1 h, showing that a mixture of Ni-rich solid solution plus the Ta-rich fcc MC phase was formed.

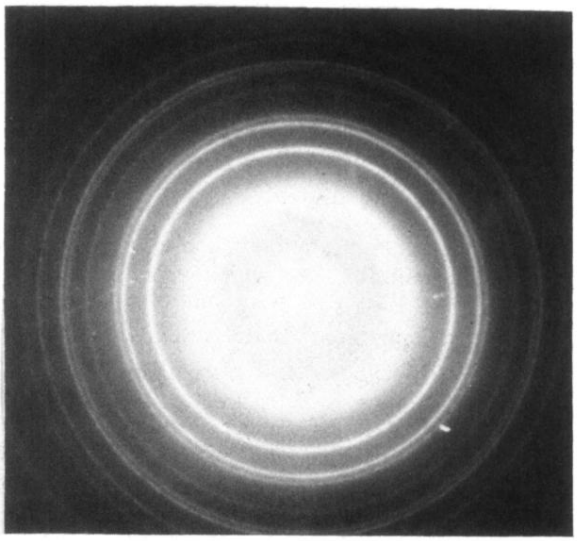

FIG. 6. Upon 450 °C annealing for half an hour, the SAD pattern shows vitrification of the fcc MC phase that was formed in the $Ni_{35}Ta_{65}$ films by RT 200-keV xenon mixing at a dose of 7×10^{14} Xe^{+}/cm^{2}.